Vector field path following and obstacle avoidance singularity mitigation via look-ahead flight envelope

First A. Author* and Second B. Author Jr.†
Business or Academic Affiliation 1, City, State, Zip Code

Unmanned Aerial Vehicles conventionally navigate by following a series of pre-planned waypoints that may have to be re-planned when flying in a dynamic environment or encountering previously unknown obstacles. Waypoints are generally planned off-line and relayed to the UAV, taking up time and autopilot communication resources. Attractive path following and repulsive obstacle avoidance vector fields have been summed together to produce UAV guidance that follows pre-planned paths and avoids obstacles without the need to re-plan. Summing attractive and repulsive vector fields may produce small regions of null guidance, called singularities, which could potentially lead to trap situations. An investigation into singularity mitigation by vector field weight parameterization is presented.

I. Nomenclature

UAV = Unmanned Aerial Vehicle

VF = Vector Field

VFF = Virtual Force Field

LVF = Lyapunov Vector Field

GVF = Goncalves Vector Field

II. Introduction

Unmanned Aerial Vehicles are pilotless aircraft used by military, police, and civilian communities for tasks such as reconnaissance, damage assessment, natural disaster surveying, and target tracking [1, 2]. Tasks can be performed by a single UAV or with a team of other air, ground, or marine vehicles [3–5]. Autonomous vehicle missions are typically accomplished by navigating a series of waypoints [1] or path following [6]. Waypoints are conventionally generated off-line at a ground station and relayed over radio to the UAVs autopilot. Obstacles such as buildings, terrain, and other vehicles can be avoided by planning waypoints around obstacles. The on-board guidance directs the UAV towards the

*Insert Job Title, Department Name, Address/Mail Stop, and AIAA Member Grade (if any) for first author.
†Insert Job Title, Department Name, Address/Mail Stop, and AIAA Member Grade (if any) for second author.

current active waypoint, once the UAV has reached a pre-defined distance from the waypoint the UAV is directed to the next waypoint. An example of a UAV following waypoint guidance while avoiding an obstacle is shown in Figure 1

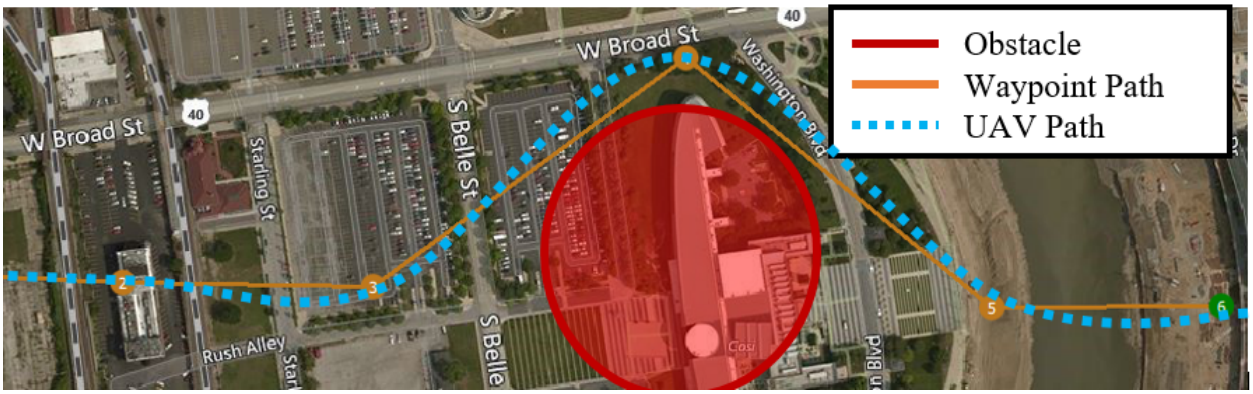

Fig. 1 UAV path from waypoint guidance

During waypoint navigation the UAV may encounter obstacles or environmental changes that would require a new set of obstacle free waypoints to be generated. For highly uncertain or dynamic environments, there may have to be frequent updates which increases the communication overhead of the autopilot. Additionally, if communication is delayed or lost, waypoints may not be updated rapidly enough and the UAV may fail to avoid the obstacles.

Obstacle free paths in static and dynamic environments have been generated with the potential field method, which models a robot's workspace as a gradient of artificial attractive and repulsive forces [7]. Potential field combines path planning, trajectory planning, and control into a single system [8]. Paths can be generated by placing a point mass at an initially high potential and allowing it to descend a gradient until the point reaches the goal, located at a global minimum potential. Obstacles provide a limited repulsive force, pushing the mass away from the obstacle.

A histogram based potential field method can be found in [9–11] which allowed for real time goal seeking with obstacle avoidance. Sensors on-board a ground robot located at (x_0, y_0) detect obstacles within a pre-defined window containing a fixed number of cells. Cells containing an obstacle provide a repulsive force $\overrightarrow{F_{i,j}}$ opposite in direction to the line-of-sight from vehicle to cell location (x_i, y_j), where (i, j) represents the cell index, F_{cr} is a constant repulsive force, W the vehicle's width, $C_{i,j}$ a cell's certainty, and $d_{i,j}$ the distance to the center of the cell with respect to robots center.

$$\overrightarrow{F_{i,j}} = \frac{F_{cr} W^n C_{i,j}}{d_{i,j}^n} \left(\frac{x_i - x_0}{d_{i,j}} \hat{x} + \frac{y_i - y_0}{d_{i,j}} \hat{y} \right) \tag{1}$$

The total repulsive force exerted on the robot is determined by summing the active cells, shown in Equation 2

$$\overrightarrow{F_r} = \sum_{i,j} \overrightarrow{F_{i,j}} \tag{2}$$

The robot is attracted to the goal by force $\overrightarrow{F_t}$ with constant magnitude F_{ct} and along the LOS from robot center to

goal, located at (x_t, y_t) and a distance d_t, shown in Equation 3

$$\overrightarrow{F_t} = F_{ct}\left(\frac{x_t - x_0}{d_t}\hat{x} + \frac{y_t - y_0}{d_t}\hat{y}\right) \tag{3}$$

Summing together attractive and repulsive forces produce a vector that can be used for heading guidance, shown in Equation 4

$$\overrightarrow{R} = \overrightarrow{F_r} + \overrightarrow{F_t} \tag{4}$$

Major drawbacks to potential field were identified in [11] consisting of local minimum and oscillations in corridors. The local minimum problem occurs when closely spaced obstacle's potential combine to produce a well on the descent gradient where a pre-mature stable point is found. Proposed solutions to local minimum include object clustering and virtual waypoint method [12], virtual escaping route [13], and use of navigation functions [14]. Oscillations in potential field were studied in [15] and [16].

In addition to local minimum and oscillations, potential field converges to a singular point which is not possible for fix wing aircraft. Similar to conventional waypoint guidance, the active goal point would change as a function of proximity. Simulating a UAV using VFF as guidance for a Dubins vehicle was performed and is shown in Figure 2, where a single obstacle cell located at the origin. The UAV initially travels directly toward the goal located at $(20, 0)$ until the obstacle is encountered, at which point a repulsive force is applied. The UAV avoids the obstacle, however significantly deviates and fails to get back on the path between waypoints. For certain applications, such as following a curved ground track, surveying, or target following, it may be beneficial to follow an explicit path.

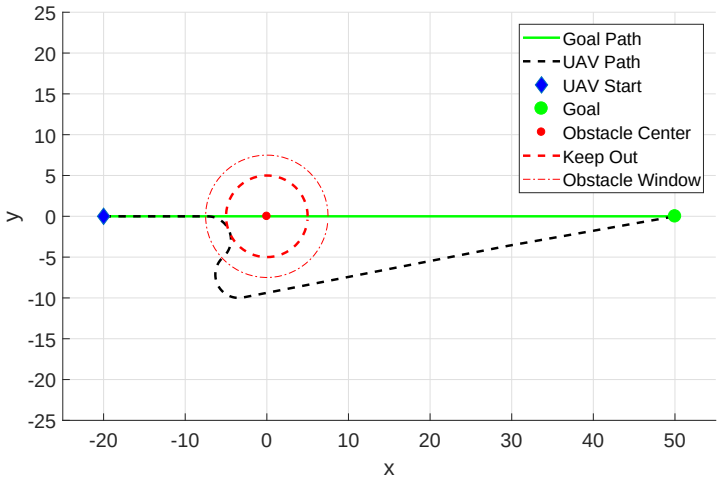

Fig. 2 Dubins vehicle encountering an obstacle while navigating to a waypoint

Path following can be accomplished with vector fields which produce a heading guidance that asymptotically

converges and circulates a path. A comparison between vector field and waypoint guidance techniques was presented in [17] where each method was evaluated based on its complexity, robustness, and accuracy. Vector field produced guidance that was both robust to external wind disturbances while maintaining a low cross track error. The two most prominent methods for generating vector fields in literature consist of the Lyapunov [18–23] and Goncalves [24–27] method.

Lyapunov vector fields for converging and following straight and circular paths were described in [18]. For converging and following a straight path, a guidance vector χ^d is determined in Equation 5, where χ^∞ is the course approach angle, y is the lateral distance to the path, and k is a positive constant that determines the rate of transition between convergence and following. An example of a Lyapunov vector field converging and following a straight line is shown in Figure 3a.

$$\chi^d(y) = -\chi^\infty \frac{2}{\pi} \tan^{-1}(ky) \tag{5}$$

For converging and following a circular path, a guidance vector χ^d is determined in Equation 6, where γ is the UAVs angular position with respect to the circle, r is the paths radius, d is the distance from the circles center, and k is a positive constant that determines the transition behavior. An example of a Lyapunov vector field for converging and following a circular path is shown in Figure 3b.

$$\chi^d(d) = \gamma - \frac{\pi}{2} - \tan^{-1}\left(k\frac{d-r}{r}\right) \tag{6}$$

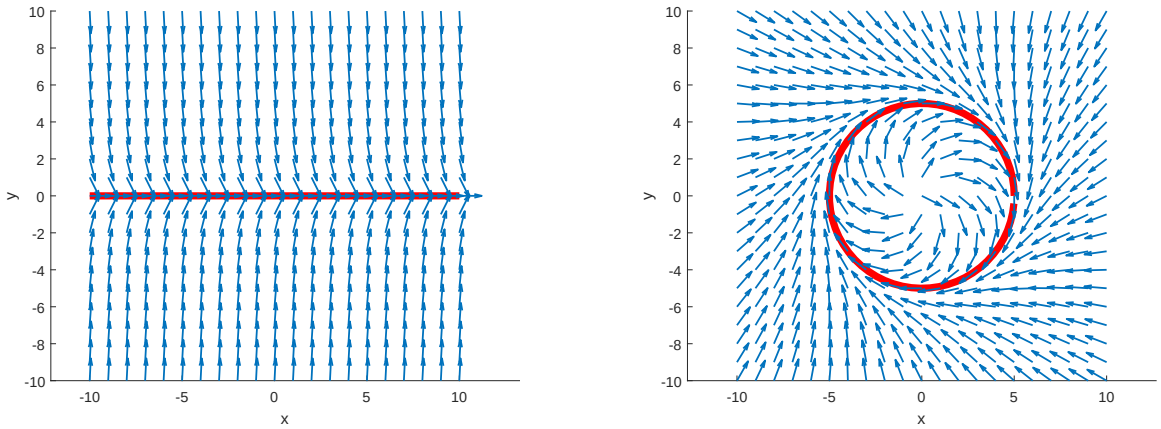

Fig. 3 Lyapunov vector field converging and following a) straight path b) circular path

Straight and circular path vector fields can be selectively activated throughout flight to form more complex paths, shown in [18–20, 28]. Lyapunov vector field for curved path following was presented in [23] which may allow for more complex paths and eliminates the need to switch between vector fields.

The Gonvalves Vector Field (GVF) method produces a similar field, however has several advantages over LVFs. GVF produces an n-dimensional vector field that converges and circulates to both static and time varying paths. Additionally, convergence, circulation, and time-varying terms that make up the GVF are decoupled from each other allowing for easy weighting of the total field. GVFs converge and circulate at the intersection, or level set, of $n-1$ dimensional implicit surfaces ($\alpha_i : \mathbb{R}^n \rightarrow \mathbb{R} | i = 1, ..., n-1$). The integral lines of the field are guaranteed to converge and circulate the level set when two conditions are met: 1) the implicit surface functions are positive definite and 2) have bounded derivatives. Consider the space with dimensions in set $\mathbf{q}$:

$$\mathbf{q} = \begin{bmatrix} x_1, x_2, ..., x_n \end{bmatrix} \tag{7}$$

The total vector field $\overrightarrow{V}$ is calculated by:

$$\overrightarrow{V} = G\nabla V + H \wedge_{i=1}^{n-1} \nabla_q \alpha_i - LM(\alpha)^{-1} a(\alpha) \tag{8}$$

or in component form:

$$\vec{V} = \vec{V}_{conv} + \vec{V}_{circ} + \vec{V}_{tv} \tag{9}$$

where $\vec{V}_{conv}$ produces vectors perpendicular to the path, $\vec{V}_{circ}$ produces vectors parallel to the path, and $\vec{V}_{tv}$ is a feed-forward term that produces vectors accounting for a time varying path.

Convergence is calculated by:

$$\vec{V}_{conv} = G\nabla V \tag{10}$$

where scalar G is multiplied by the gradient of the definite potential function V:

$$V = -\sqrt{{\alpha_1}^2 + {\alpha_2}^2} \tag{11}$$

Circulation is calculated by taking the wedge product of the gradient:

$$\vec{V}_{circ} = \wedge_{i=1}^{n-1} \nabla_q \alpha_i \tag{12}$$

In the case of ($n = 3$) the wedge product simplifies as the cross product:

$$\vec{V}_{circ} = \nabla_q \alpha_1 \times \nabla_q \alpha_2 \tag{13}$$

The feed-forward time-varying component is calculated by:

$$\vec{V}_{tv} = M^{-1} a \tag{14}$$

where,

$$M = \begin{bmatrix} \nabla \alpha_1^T \\ \nabla \alpha_2^T \\ (\nabla \alpha_1 \times \nabla \alpha_2)^T \end{bmatrix} \tag{15}$$

$$a = \begin{bmatrix} \frac{\partial \alpha_1}{\partial t} & \frac{\partial \alpha_2}{\partial t} & 0 \end{bmatrix}^T \tag{16}$$

Intersecting two flat planes ($\alpha_1 = z, \alpha_2 = x$) produces a GVF that converges and circulates a straight path, shown in Figure 5. A circular path can be produced by intersecting a plane and a cylinder ($\alpha_1 = z, \alpha_2 = x^2 + y^2 - r^2$).

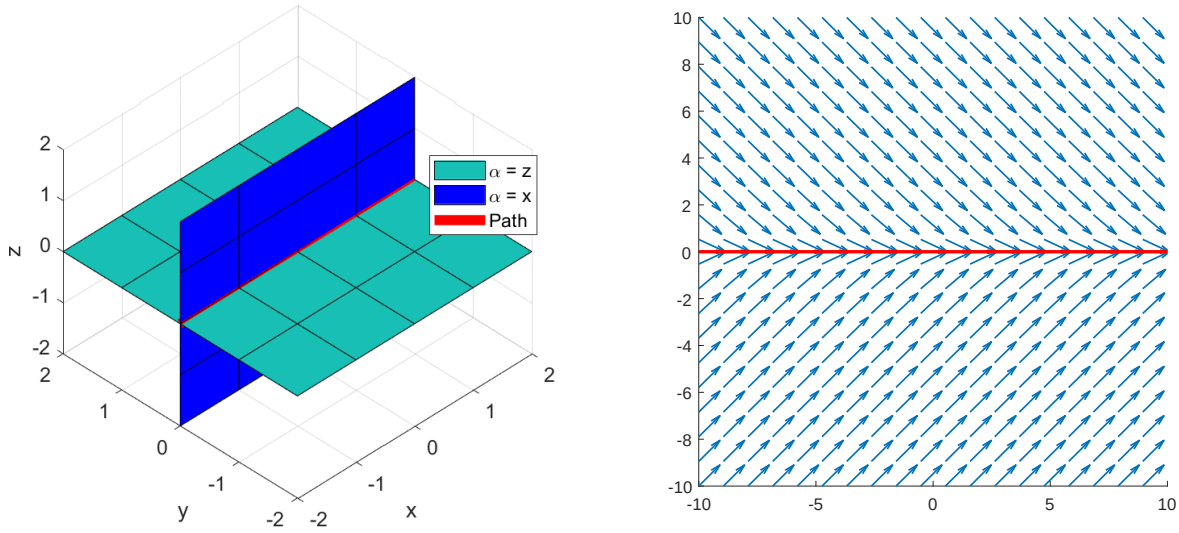

(a) (b)

Fig. 4 GVF converging and circulating straight path

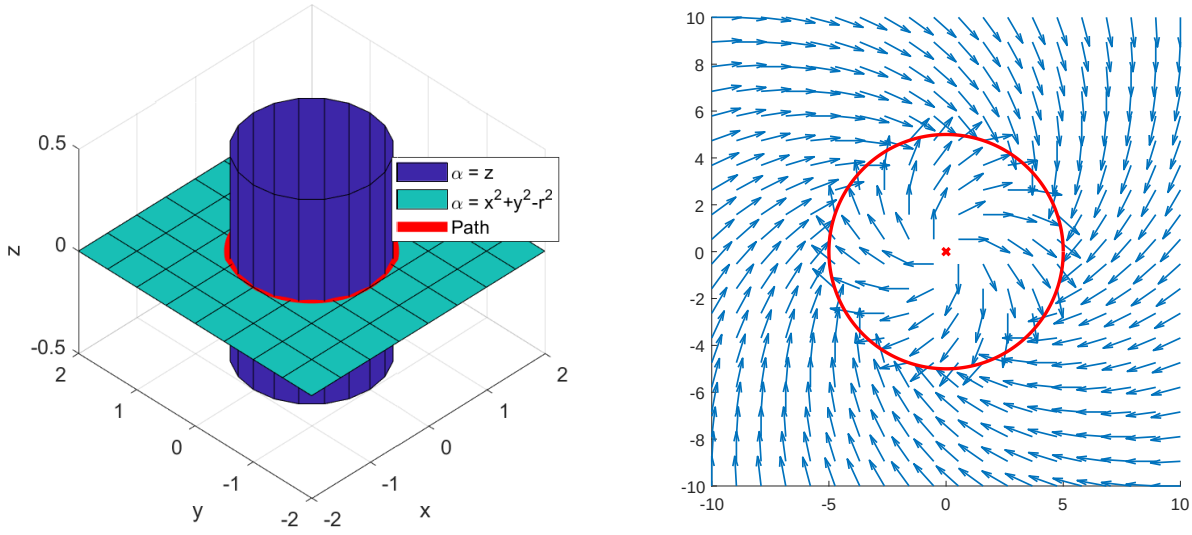

(a) (b)

Fig. 5 GVF converging and circulating circular path

The standoff tracking scenario presented in [Wilhelm] tasked a fixed wing UAV with loitering around a moving ground target while adding obstacle avoidance constraints. A circular attractive vector field was attached to a moving ground target. Repulsive vector fields centered at the obstacles and weighted by hyperbolic tangent decay functions were summed with the attractive circular field to produce a target loitering and obstacle avoidance guidance. The performance of Lyapunov [21] and gradient vector field [24–26] were compared for their cross track error with respect to the loiter circle. Gradient vector field had favorable performance due to compensation for a time-varying vector field. The gradient vector field technique also has the benefit of decoupled weighting parameters for convergence, circulation, and time-varying terms, allowing for easy modification of field behavior.

Decay functions for avoidance fields using GVF were investigated in [Zhu] for obstacles present on a straight path. When summing attractive and repulsive vector fields there is the possibility of guidance singularities, where magnitude and direction are equal and opposite. The presence of singularities were not addressed in [Wilhelm] and [Zhu], mentioned briefly in [18] and observed in [29]. For fixed wing UAVs the lack of guidance may prevent the UAV from avoiding an obstacle, while multi-rotor UAVs may end up in a trap situation. Singularities may be present at any location where a goal field and obstacle field are of equal strength.

Dubin's vehicle's position $\overrightarrow{X}$ at time t is calculated from the integral of the velocity vector $\overrightarrow{U}$. The vehicle has a constant velocity magnitude u_{uav} at a heading θ. The rate at which θ changes with respect to time is based on limitations

of the craft itself.

$$\overrightarrow{U}(t) = u_{uav} \begin{bmatrix} cos(\theta(t)) \\ sin(\theta(t)) \end{bmatrix} \tag{17}$$

$$\overrightarrow{X}(t) = \overrightarrow{U} dt + \overrightarrow{X}(t-1) \tag{18}$$

$$\dot{\theta} \leq 20 deg/s \tag{19}$$

III. methods

Overview of methods

Construction of guidance for desired path

Construction of avoidance guidance

Path following and obstacle avoidance guidance

Singularity detection

Selection of vf parameters for optimized obstacle avoidance

A. Path Following

Path following guidance for a planar UAV at position (x, y) for a time invariant line is achieved by summing together convergence $\overrightarrow{V}_{conv}$ and circulation $\overrightarrow{V}_{circ}$ terms shown in Equation 20.

$$\overrightarrow{V} = \overrightarrow{V}_{conv} + \overrightarrow{V}_{circ} \tag{20}$$

where

$$\overrightarrow{V}_{conv} = G \nabla V \tag{21}$$

and the potential function V is

$$V = -\sqrt{\alpha_1^2 + \alpha_2^2} \tag{22}$$

where the plane defined by implicit surface function α_1 is at angle θ and plane α_2 is at constant height of $Z = 1$ shown in Equations 23 and 24 respectively.

$$\alpha_1 = cos(\theta)x + sin(\theta)y \tag{23}$$

$$\alpha_2 = z \tag{24}$$

The gradient ∇ of implicit function V is shown in Equation 25.

$$\nabla V = -\frac{1}{2(\sqrt{\cos^2\theta x^2 + 2\cos\theta\sin\theta xy + \sin^2\theta y^2})} \begin{bmatrix} 2x\cos^2\theta + 2\cos\theta\sin\theta y \\ 2y\sin^2\theta + 2\cos\theta\sin\theta x \\ 2z \end{bmatrix} \tag{25}$$

Circulation is calculated by the cross product of the functions α_1 and α_2, shown in Equation 26 and 27.

$$\overrightarrow{V}_{circ} = \nabla\alpha_1 \times \nabla\alpha_2 \tag{26}$$

$$\overrightarrow{V}_{circ} = \begin{bmatrix} cos(\theta) \\ sin(\theta) \\ 0 \end{bmatrix} \tag{27}$$

Guidance for a path at angle $\theta = 0$ and equal parts circulation and convergence weights $G = H = 1$ is shown in Figure 6 below.

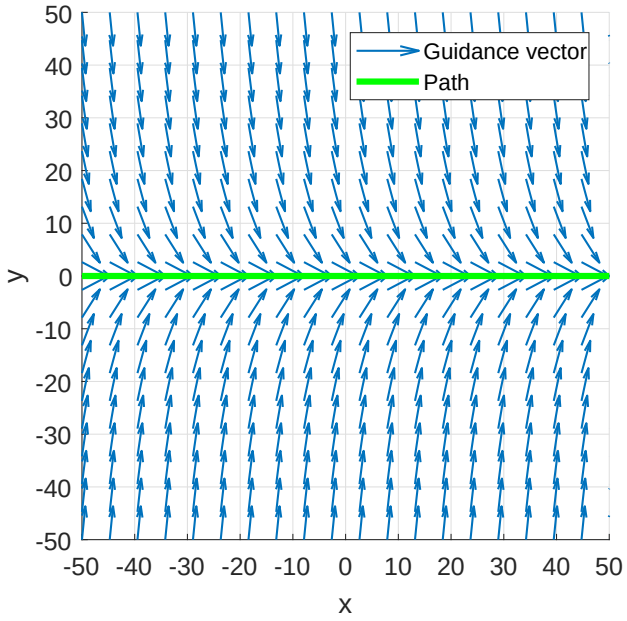

Fig. 6

B. Avoidance

Constructing a repulsive vector field for avoidance using the GVF method starts with constructing a vector field that converges and circulates a circular path. A GVF that converges and circulates a circular path is constructed with the implicit functions of a cylinder of radius r centered at (x_c, y_c) and a level plane of constant height Z, shown in Equations 28 and 29 below.

$$\alpha_1 = (x - x_c)^2 + (y - y_c)^2 - r^2 \tag{28}$$

$$\alpha_2 = z \tag{29}$$

Convergence is determined by the gradient of the potential function 25, which when simplified evaluates to

$$\overrightarrow{V}_{conv} = A\overrightarrow{B} \tag{30}$$

where

$$A = \frac{-1}{\sqrt{\bar{x}^4 + \bar{y}^4 + 2\bar{x}^2\bar{y}^2 - 2r^2\bar{x}^2 - 2r^2\bar{y}^2 + r^2 + z^2}} \tag{31}$$

and

$$\overrightarrow{B} = \begin{bmatrix} 2\bar{x}^3 + 2\bar{x}\bar{y}^2 - 2r^2\bar{x} \\ 2\bar{y}^3 + 2\bar{x}^2\bar{y} - 2r^2\bar{y} \\ z \end{bmatrix} \tag{32}$$

.

$$\bar{x} = x - x_c \tag{33}$$

$$\bar{y} = y - y_c \tag{34}$$

Circulation is calculated from the cross product of each implicit surface functions gradient, which simplifies to

$$\overrightarrow{V}_{circ} = \begin{bmatrix} 2(y - y_c) \\ -2(x - x_c) \\ 0 \end{bmatrix} \tag{35}$$

Guidance for avoiding a circular path with a large radius can be produced by setting the convergence weight $G = -1$ and circulation weight $H = 0$, shown in Figure 7.

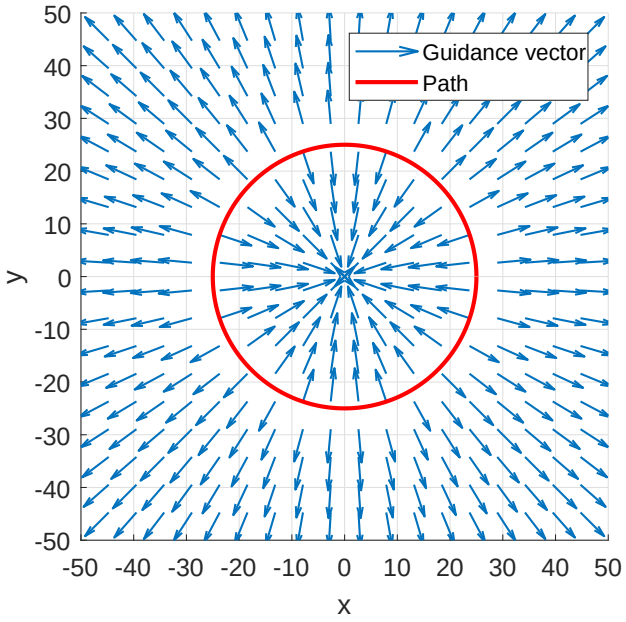

Fig. 7

Note that inside of the path, vectors point towards the center of the circle which may produce a trap situation if the

UAV ends up inside the radius. To prevent a trap situation inside of the circular path, the radius of the path can be reduced, as shown in Figure 8 where $r = 0.01$.

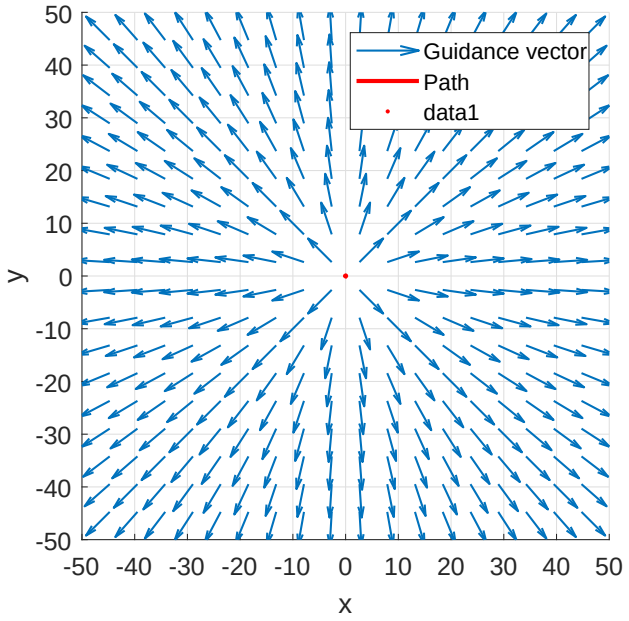

Fig. 8

Before summing obstacle avoidance with the path following guidance a decay function is applied to the repulsive field to limit the fields influence to within a radius R. The decay strength P is determined in 36, where d is the euclidean distance, or range, between the UAV and the center of the obstacle, shown in Equation 37.

$$P = -\tanh\left(\frac{2\pi d}{R} - \pi\right) + 1 \tag{36}$$

$$d = \sqrt{\bar{x}^2 + \bar{y}^2} \tag{37}$$

Applying the decay function with a decay edge radius $R = 35$ to the GVF shown in figure 8, results in the field shown in Figure 9.

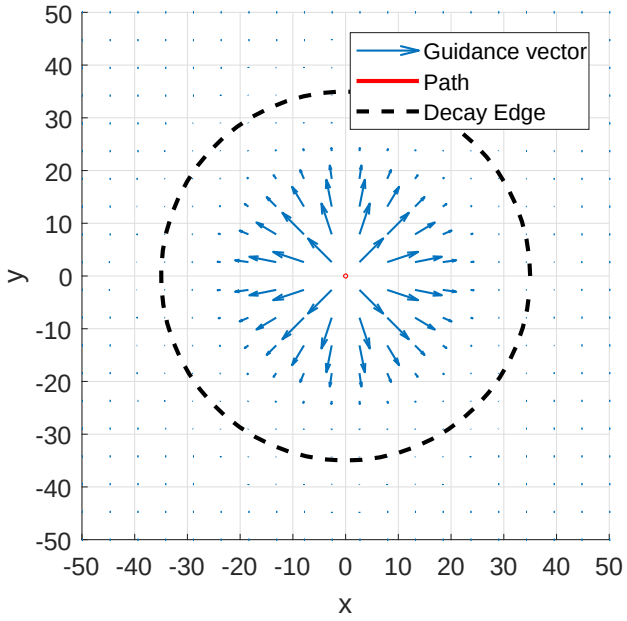

Fig. 9

Summing together path following field with an obstacle centered on the path results in the guidance shown in Figure 10.

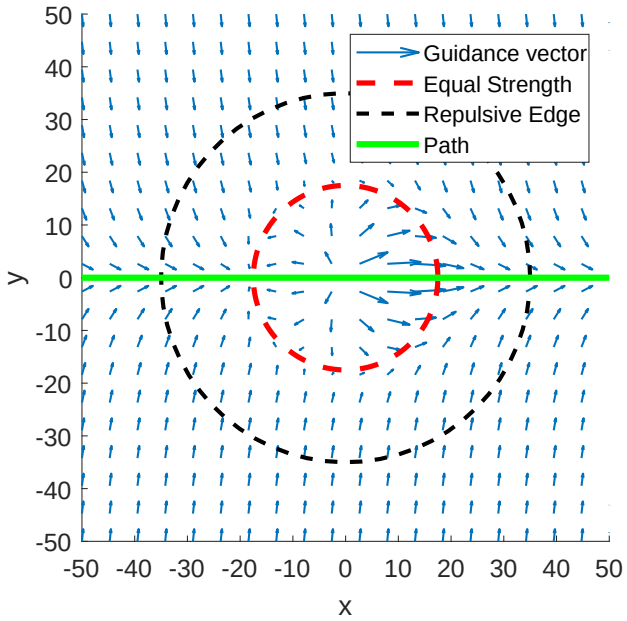

Fig. 10

Summing GVFs together may lead to small regions where the vector magnitude is near or equal to zero

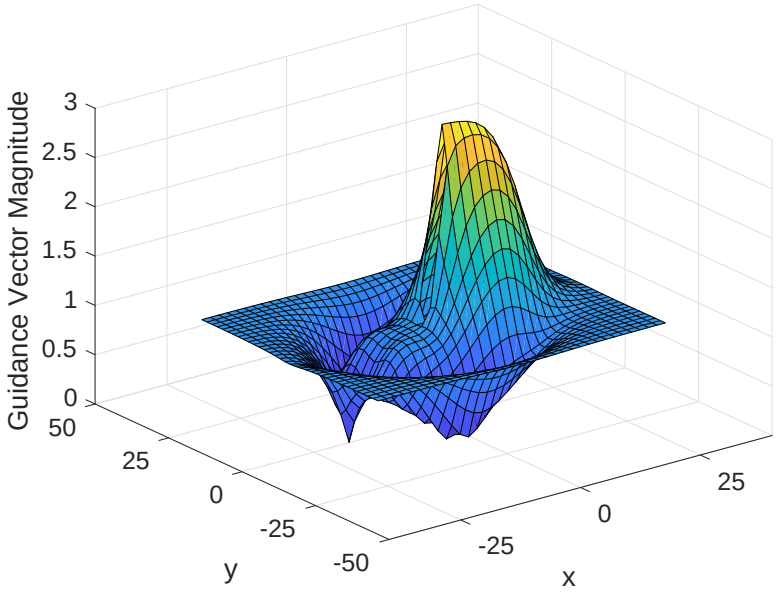

Fig. 11

$$\overrightarrow{V}_g = \overrightarrow{V}_{path} + P\overrightarrow{V}_{obst} \tag{38}$$

$$||\overrightarrow{V}_g|| = 0 \tag{39}$$

C. Flight Envelope

$$\overrightarrow{X} = \begin{bmatrix} x & y & 0 \end{bmatrix}^T \tag{40}$$

$$\overrightarrow{X_b} = \frac{u}{\dot{\theta}} \begin{bmatrix} \sin(t_h\dot{\theta}) \\ (1-\cos(t_h\dot{\theta}) \\ 0 \end{bmatrix} \tag{41}$$

$$q = ||\overrightarrow{X_b}|| \tag{42}$$

$$\phi = \tan^{-1}\left(\frac{y_b}{x_b}\right) \tag{43}$$

$$\overrightarrow{q_b} = \begin{bmatrix} q\cos\phi \\ q\sin\phi \\ 0 \end{bmatrix} \tag{44}$$

$$R_b^0 = \begin{bmatrix} \cos(\theta) & -\sin(\theta) & 0 \\ \sin\theta & \cos\theta & 0 \\ 0 & 0 & 1 \end{bmatrix} \tag{45}$$

$$\overrightarrow{Q}_0 = \overrightarrow{P} + R_b^0 \overrightarrow{q_b} \tag{46}$$

IV. Conclusion

Appendix

Acknowledgments

References

[1] Ariyur, K. B., and Fregene, K. O., "Autonomous tracking of a ground vehicle by a UAV," *American Control Conference, 2008*, IEEE, 2008, pp. 669–671.

[2] Teuliere, C., Eck, L., and Marchand, E., "Chasing a moving target from a flying UAV," *Intelligent Robots and Systems (IROS), 2011 IEEE/RSJ International Conference on*, IEEE, 2011, pp. 4929–4934.

[3] Oh, H., Kim, S., Shin, H.-S., Tsourdos, A., and White, B., "Coordinated standoff tracking of groups of moving targets using multiple UAVs," *Control & Automation (MED), 2013 21st Mediterranean Conference on*, IEEE, 2013, pp. 969–977. URL http://ieeexplore.ieee.org/abstract/document/6608839/.

[4] Hyondong Oh, Seungkeun Kim, Hyo-sang Shin, and Tsourdos, A., "Coordinated standoff tracking of moving target groups using multiple UAVs," *IEEE Transactions on Aerospace and Electronic Systems*, Vol. 51, No. 2, 2015, pp. 1501–1514. doi:10.1109/TAES.2015.140044, URL http://ieeexplore.ieee.org/document/7126199/.

[5] Ulun, S., and Unel, M., "Coordinated motion of UGVs and a UAV," *Industrial Electronics Society, IECON 2013-39th Annual Conference of the IEEE*, IEEE, 2013, pp. 4079–4084. URL http://ieeexplore.ieee.org/abstract/document/6699789/.

[6] Oliveira, T., Aguiar, A. P., and Encarnacao, P., "Moving Path Following for Unmanned Aerial Vehicles With Applications to Single and Multiple Target Tracking Problems," *IEEE Transactions on Robotics*, Vol. 32, No. 5, 2016, pp. 1062–1078. doi:10.1109/TRO.2016.2593044, URL http://ieeexplore.ieee.org/document/7553466/.

[7] Khatib, O., "Real-time obstacle avoidance for manipulators and mobile robots," *The international journal of robotics research*, Vol. 5, No. 1, 1986, pp. 90–98. URL http://journals.sagepub.com/doi/abs/10.1177/027836498600500106.

[8] Rimon, E., "Exact Robot Navigation Using Artificial Potential Functions.pdf," , 1992.

[9] Borenstein, J., and Koren, Y., "Real-time obstacle avoidance for fast mobile robots in cluttered environments," *Robotics and Automation, 1990. Proceedings., 1990 IEEE International Conference on*, IEEE, 1990, pp. 572–577. URL http://ieeexplore.ieee.org/abstract/document/126042/.

[10] Borenstein, J., and Koren, Y., "The vector field histogram-fast obstacle avoidance for mobile robots," *IEEE transactions on robotics and automation*, Vol. 7, No. 3, 1991, pp. 278–288. URL http://ieeexplore.ieee.org/abstract/document/88137/.

[11] Koren, Y., and Borenstein, J., "Potential Field Methods and their inherent limitions for morbile robot navigation.pdf," , 1991. URL http://ieeexplore.ieee.org/document/131810/.

[12] Liu, Y., and Zhao, Y., "A virtual-waypoint based artificial potential field method for UAV path planning," *Guidance, Navigation and Control Conference (CGNCC), 2016 IEEE Chinese*, IEEE, 2016, pp. 949–953. URL http://ieeexplore.ieee.org/abstract/document/7828913/.

[13] Kim, D. H., "Escaping route method for a trap situation in local path planning," *International Journal of Control, Automation and Systems*, Vol. 7, No. 3, 2009, pp. 495–500. doi:10.1007/s12555-009-0320-7, URL http://link.springer.com/10.1007/s12555-009-0320-7.

[14] Goerzen, C., Kong, Z., and Mettler, B., "A Survey of Motion Planning Algorithms from the Perspective of Autonomous UAV Guidance," *Journal of Intelligent and Robotic Systems*, Vol. 57, No. 1-4, 2010, pp. 65–100. doi:10.1007/s10846-009-9383-1, URL http://link.springer.com/10.1007/s10846-009-9383-1.

[15] Lei Tang, Songyi Dian, Gangxu Gu, Kunli Zhou, Suihe Wang, and Xinghuan Feng, "A novel potential field method for obstacle avoidance and path planning of mobile robot," IEEE, 2010, pp. 633–637. doi:10.1109/ICCSIT.2010.5565069, URL http://ieeexplore.ieee.org/document/5565069/.

[16] Li, G., Yamashita, A., Asama, H., and Tamura, Y., "An efficient improved artificial potential field based regression search method for robot path planning," IEEE, 2012, pp. 1227–1232. doi:10.1109/ICMA.2012.6283526, URL http://ieeexplore.ieee.org/document/6283526/.

[17] Sujit, P., Saripalli, S., and Sousa, J. B., "Unmanned Aerial Vehicle Path Following: A Survey and Analysis of Algorithms for Fixed-Wing Unmanned Aerial Vehicless," *IEEE Control Systems*, Vol. 34, No. 1, 2014, pp. 42–59. doi:10.1109/MCS.2013.2287568, URL http://ieeexplore.ieee.org/document/6712082/.

[18] Nelson, D. R., "Cooperative control of miniature air vehicles," 2005. URL http://scholarsarchive.byu.edu/etd/1095/.

[19] Nelson, D. R., Barber, D. B., McLain, T. W., and Beard, R. W., "Vector field path following for small unmanned air vehicles," *American Control Conference, 2006*, IEEE, 2006, pp. 7–pp. URL http://ieeexplore.ieee.org/abstract/document/1657648/.

[20] Nelson, D., Barber, D., McLain, T., and Beard, R., "Vector Field Path Following for Miniature Air Vehicles," *IEEE Transactions on Robotics*, Vol. 23, No. 3, 2007, pp. 519–529. doi:10.1109/TRO.2007.898976, URL http://ieeexplore.ieee.org/document/4252175/.

[21] Frew, E. W., "Cooperative standoff tracking of uncertain moving targets using active robot networks," *Robotics and Automation, 2007 IEEE International Conference on*, IEEE, 2007, pp. 3277–3282. URL http://ieeexplore.ieee.org/abstract/document/4209596/.

[22] Miao, Z., Thakur, D., Erwin, R. S., Pierre, J., Wang, Y., and Fierro, R., "Orthogonal vector field-based control for a multi-robot system circumnavigating a moving target in 3D," *Decision and Control (CDC), 2016 IEEE 55th Conference on*, IEEE, 2016, pp. 6004–6009. URL http://ieeexplore.ieee.org/abstract/document/7799191/.

[23] Griffiths, S., "Vector Field Approach for Curved Path Following for Miniature Aerial Vehicles," American Institute of Aeronautics and Astronautics, 2006. doi:10.2514/6.2006-6467, URL http://arc.aiaa.org/doi/10.2514/6.2006-6467.

[24] Goncalves, V. M., Pimenta, L. C. A., Maia, C. A., and Pereira, G. A. S., "Artificial vector fields for robot convergence and circulation of time-varying curves in n-dimensional spaces," IEEE, 2009, pp. 2012–2017. doi:10.1109/ACC.2009.5160350, URL http://ieeexplore.ieee.org/document/5160350/.

[25] Gonçalves, V. M., Pimenta, L. C., Maia, C. A., Pereira, G. A., Dutra, B. C., Michael, N., Fink, J., and Kumar, V., "Circulation of curves using vector fields: actual robot experiments in 2D and 3D workspaces," *Robotics and Automation (ICRA), 2010 IEEE International Conference on*, IEEE, 2010, pp. 1136–1141.

[26] Gonçalves, V. M., Pimenta, L. C., Maia, C. A., Dutra, B. C., and Pereira, G. A., "Vector fields for robot navigation along time-varying curves in $ n $-dimensions," *IEEE Transactions on Robotics*, Vol. 26, No. 4, 2010, pp. 647–659. URL http://ieeexplore.ieee.org/abstract/document/5504176/.

[27] Gerlach, A. R., *Autonomous Path-Following by Approximate Inverse Dynamics and Vector Field Prediction*, University of Cincinnati, 2014. URL http://search.proquest.com/openview/432d738d856bf0a9b46acea1b1eee08f/1?pq-origsite=gscholar&cbl=18750&diss=y.

[28] Jung, W., Lim, S., Lee, D., and Bang, H., "Unmanned Aircraft Vector Field Path Following with Arrival Angle Control," *Journal of Intelligent & Robotic Systems*, Vol. 84, No. 1-4, 2016, pp. 311–325. doi:10.1007/s10846-016-0332-5, URL http://link.springer.com/10.1007/s10846-016-0332-5.

[29] Panagou, D., "Motion planning and collision avoidance using navigation vector fields," *Robotics and Automation (ICRA), 2014 IEEE International Conference on*, IEEE, 2014, pp. 2513–2518. URL http://ieeexplore.ieee.org/abstract/document/6907210/.